

Article

Manipulating the Conformation of 3,2':6',3''-Terpyridine in $[\text{Cu}_2(\mu\text{-OAc})_4(3,2':6',3''\text{-tpy})]_n$ 1D-Polymers

 Dalila Rocco , Samantha Novak, Alessandro Prescimone , Edwin C. Constable  and Catherine E. Housecroft * 

Department of Chemistry, University of Basel, BPR 1096, Mattenstrasse 24a, CH-4058 Basel, Switzerland; dalila.rocco@unibas.ch (D.R.); samantha.novak@stud.unibas.ch (S.N.); alessandro.prescimone@unibas.ch (A.P.); edwin.constable@unibas.ch (E.C.C.)

* Correspondence: catherine.housecroft@unibas.ch; Tel.: +41-612-071-008

Abstract: We report the preparation and characterization of 4'-([1,1'-biphenyl]-4-yl)-3,2':6',3''-terpyridine (**1**), 4'-(4'-fluoro-[1,1'-biphenyl]-4-yl)-3,2':6',3''-terpyridine (**2**), 4'-(4'-chloro-[1,1'-biphenyl]-4-yl)-3,2':6',3''-terpyridine (**3**), 4'-(4'-bromo-[1,1'-biphenyl]-4-yl)-3,2':6',3''-terpyridine (**4**), and 4'-(4'-methyl-[1,1'-biphenyl]-4-yl)-3,2':6',3''-terpyridine (**5**), and their reactions with copper(II) acetate. Single-crystal structures of the $[\text{Cu}_2(\mu\text{-OAc})_4\text{L}]_n$ 1D-coordination polymers with L = 1–5 have been determined, and powder X-ray diffraction confirms that the single crystal structures are representative of the bulk samples. $[\text{Cu}_2(\mu\text{-OAc})_4(\mathbf{1})]_n$ and $[\text{Cu}_2(\mu\text{-OAc})_4(\mathbf{2})]_n$ are isostructural, and zigzag polymer chains are present which engage in π -stacking interactions between [1,1'-biphenyl]pyridine units. 1D-chains nest into one another to give 2D-sheets; replacing the peripheral H in **1** by an F substituent in **2** has no effect on the solid-state structure, indicating that bifurcated contacts (H...H for **1** or H...F for **2**) are only secondary packing interactions. Upon going from $[\text{Cu}_2(\mu\text{-OAc})_4(\mathbf{1})]_n$ and $[\text{Cu}_2(\mu\text{-OAc})_4(\mathbf{2})]_n$ to $[\text{Cu}_2(\mu\text{-OAc})_4(\mathbf{3})]_n$, $[\text{Cu}_2(\mu\text{-OAc})_4(\mathbf{4})]_n$, and $[\text{Cu}_2(\mu\text{-OAc})_4(\mathbf{5})]_n \cdot n\text{MeOH}$, the increased steric demands of the Cl, Br, or Me substituent induces a switch in the conformation of the 3,2':6',3''-tpy metal-binding domain, and a concomitant change in dominant packing interactions to py–py and py–biphenyl face-to-face π -stacking. The study underlines how the 3,2':6',3''-tpy domain can adapt to different steric demands of substituents through its conformational flexibility.

Keywords: 3,2':6',3''-terpyridine; coordination polymer; copper(II) acetate; paddle-wheel building block; X-ray diffraction



Citation: Rocco, D.; Novak, S.; Prescimone, A.; Constable, E.C.; Housecroft, C.E. Manipulating the Conformation of 3,2':6',3''-Terpyridine in $[\text{Cu}_2(\mu\text{-OAc})_4(3,2':6',3''\text{-tpy})]_n$ 1D-Polymers. *Chemistry* **2021**, *3*, 182–198. <https://doi.org/10.3390/chemistry3010015>

Received: 11 December 2020

Accepted: 26 January 2021

Published: 2 February 2021

Publisher's Note: MDPI stays neutral with regard to jurisdictional claims in published maps and institutional affiliations.

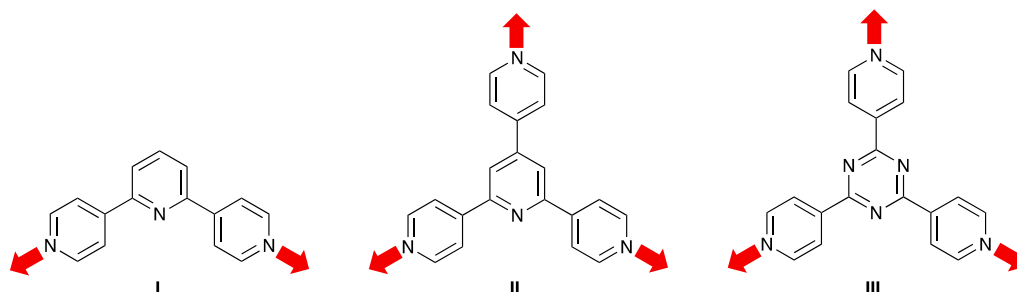


Copyright: © 2021 by the authors. Licensee MDPI, Basel, Switzerland. This article is an open access article distributed under the terms and conditions of the Creative Commons Attribution (CC BY) license (<https://creativecommons.org/licenses/by/4.0/>).

1. Introduction

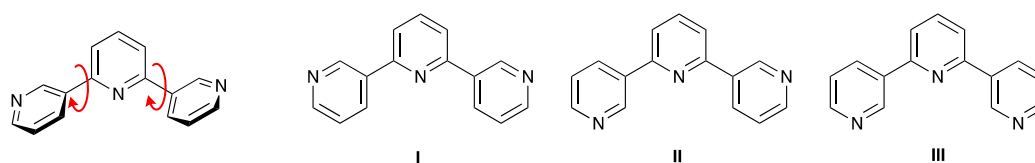
For many chemists, the word “terpyridine” is synonymous with 2,2':6',2''-terpyridine (tpy), the coordination chemistry and applications of which are exceptionally well developed [1–5]. However, from the perspective of assembling coordination polymers and networks, the bis-chelating nature of tpy tends to restrict its use to $\{M(\text{tpy})_2\}$ units bearing peripheral functionalities that can act as metal-binding domains or polytopic ligands containing multiple tpy metal-binding domains. Such “expanded ligands” with the $\{M(\text{tpy})_2\}$ unit on the “inside” of the metalloligand have gained significant attention [6]. Ditopic bis(tpy) ligands designed to assemble metallomacrocycles with predetermined internal angles feature in the innovative work of Newkome and coworkers [7]. However, while retaining a terpyridine building block, the most efficient way to access 1D-coordination polymers and 2D- and 3D-coordination networks is to turn to other isomers of terpyridine [8]. The 4,2':6',4''- and 3,2':6',3''-isomers are synthetically accessible using either Kröhnke methodology [9] or the one-pot approach of Wang and Hanan [10]. Over the last decade, the coordination chemistry of 4,2':6',4''-terpyridines (4,2':6',4''-tpy (**I**), Scheme 1) has gained in popularity [8]. Functionalization in the 4'-position with coordinatively non-innocent substituents increases the connectivity of the building block, taking it from a V-shaped linker to a 3- (or higher) connecting node. It is noteworthy that the introduction

of a 4'-(pyridin-4-yl) unit (**II**, Scheme 1) produces a 3-connecting building block analogous to 2,4,6-tris(pyridinyl)-1,3,5-triazine (**III**, Scheme 1) employed by Fujita and coworkers for the assembly of molecular capsules [11]. Like the nitrogen atoms of the triazine ring, the N-atom of the central pyridine in 4,2':6',4''-tpy does not bind a metal ion. The same is true in 3,2':6',3''-terpyridine (3,2':6',3''-tpy).



Scheme 1. 4,2':6',4''-Terpyridine as a ditopic ligand (**I**), and 4'-(pyridin-4-yl)-4,2':6',4''-terpyridine (**II**) as a 3-connecting building block compared to 2,4,6-tris(pyridinyl)-1,3,5-triazine (**III**).

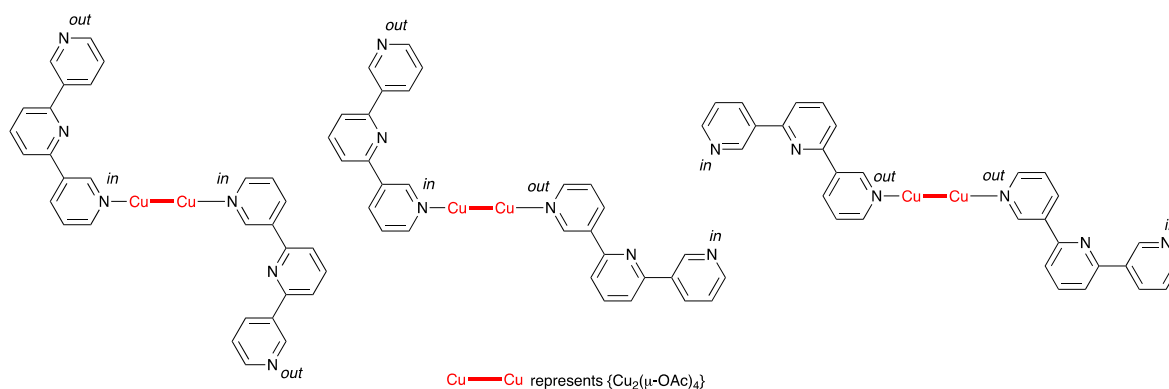
The coordination chemistry of 3,2':6',3''-tpy has received less attention than that of the 4,2':6',4''-isomer [8]. One aspect of 3,2':6',3''-tpy that makes predictive crystal engineering difficult is that rotation about the inter-ring C–C bonds (Scheme 2) leads to different ligand conformations and, therefore, to variable vectorial properties of the ditopic ligand. Scheme 2 illustrates the three possible planar conformations of 3,2':6',3''-tpy. We have recently demonstrated conformational switching in free 4'-(4-*n*-alkyloxyphenyl)-3,2':6',3''-terpyridines [12], and in $[\text{Cu}_2(\mu\text{-OAc})_4\text{L}]_n$ 1D-chains [13] and $[\text{Co}(\text{NCS})_2\text{L}_2]_n$ 2D-networks where L is a 4'-(4-*n*-alkyloxyphenyl)-3,2':6',3''-tpy [14,15] as a function of the alkyloxy chain length. In these structures, the 3,2':6',3''-tpy domain adopts either conformation **I** or **II** (Scheme 2). Although conformation **III** is suited to the formation of discrete molecular architectures [16–20], it also appears in several infinite assemblies [21–24]. In one 3D-assembly, the 3,2':6',3''-tpy domain is locked into conformation **III** by virtue of a bridging cyano ligand between the coordinated metal centres of a single 3,2':6',3''-tpy unit, and propagation of the coordination network into 3-dimensions relies on the presence of a 4'-pyridin-4-yl substituent [25].



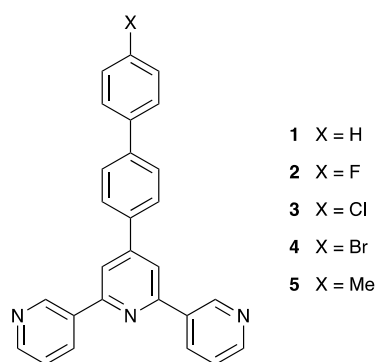
Scheme 2. Rotation about the inter-ring C–C bonds in 3,2':6',3''-tpy leads to three planar conformations **I–III**.

In the $[\text{Cu}_2(\mu\text{-OAc})_4\{4'-(4\text{-}n\text{-alkyloxyphenyl})\text{-}3,2':6',3''\text{-tpy}\}]_n$ 1D-polymers with alkyloxy groups being methoxy, butyloxy, pentyloxy, hexyloxy, or heptyloxy [13,26], the conformational variation is more complex than a switch from **I** to **II** [13]. With the ligand in conformation **II**, the arrangement in the two axial sites of the $\{\text{Cu}_2(\mu\text{-OAc})_4\}$ paddlewheel [27] can follow one of three assembly algorithms as shown in Scheme 3. The labels *in* and *out* refer to the orientation of the lone pair of each coordinating N atom with respect to the central N atom of the 3,2':6',3''-tpy unit. Both *in/out/in/out...* and *out/out/in/in...* sequences are observed in $[\text{Cu}_2(\mu\text{-OAc})_4\{4'-(4\text{-}n\text{-alkyloxyphenyl})\text{-}3,2':6',3''\text{-tpy}\}]_n$ chains, and we have proposed that this is related to the growing importance of inter-chain van der Waals forces as the length of the alkyloxy chain increases. These interactions complement π -stacking interactions between phenyl/pyridine and pyridine/pyridine rings [13]. Following from these results, we were interested in exploring the effects of replacing the alkyloxy tails by substituents in which π -stacking interactions would be dominant.

We chose to focus on the 3,2':6',3''-tpy ligands featuring 1,1'-biphenyl units, and selected ligands 1–5 (Scheme 4). We have previously observed that π -stacking between pairs of 1,1'-biphenyl units in the solid state structures of 1D-coordination polymers involving 4'-([1,1'-biphenyl]-4-yl)-4,2':6',4''-tpy ligands is a dominant packing interaction, even when the peripheral phenyl ring is perfluorinated [28,29].



Scheme 3. In conformation II, there are three arrangements of the 3,2':6',3''-tpy units in the axial sites of the $\{Cu_2(\mu-OAc)_4\}$ unit if the two ligands are coplanar.



Scheme 4. Structures of ligands 1–5.

2. Materials and Methods

2.1. General

1H , $^{13}C\{^1H\}$, $^{19}F\{^1H\}$, and 2D NMR spectra were recorded on a Bruker Avance III-500 spectrometer equipped with a BBFO probehead (Bruker BioSpin AG, Fällanden, Switzerland) at 298 K. The 1H and ^{13}C NMR chemical shifts were referenced with respect to residual solvent peaks (δ TMS = 0). A Shimadzu LCMS-2020 instrument (Shimadzu Schweiz GmbH, Roemerstr., Switzerland) was used to record electrospray ionization (ESI) mass spectra. A PerkinElmer UATR Two instrument (Perkin Elmer, 8603 Schwerzenbach, Switzerland) was used to record FT-infrared (IR) spectra, and a Shimadzu UV2600 (Shimadzu Schweiz GmbH, 4153 Reinach, Switzerland) spectrophotometer was used to record absorption spectra. 3-Acetylpyridine and [1,1'-biphenyl]-4-carbaldehyde were purchased from Acros Organics (Fisher Scientific AG, 4153 Reinach, Switzerland), 4'-chloro-[1,1'-biphenyl]-4-carbaldehyde and 4'-methyl-[1,1'-biphenyl]-4-carbaldehyde from Fluorochem (Chemie Brunschwig AG, 4052 Basel, Switzerland), 4'-fluoro-[1,1'-biphenyl]-4-carbaldehyde from Combi-Blocks (Chemie Brunschwig AG, 4052 Basel, Switzerland), and 4'-bromo-[1,1'-biphenyl]-4-carbaldehyde from Apollo (Chemie Brunschwig AG, 4052 Basel, Switzerland). Copper(II) acetate monohydrate was bought from Fluka (Fluka Chemie GmbH, 9471 Buchs, Switzerland). All chemicals were used as received.

All single-crystal growth experiments were carried out under ambient conditions using identical crystallization tubes (i.d. = 13.6 mm, 24 mL).

2.2. Compound 1

[1,1'-Biphenyl]-4-carbaldehyde (1.84 g, 10.0 mmol) was dissolved in EtOH (50 mL), and then 3-acetylpyridine (2.42 g, 2.20 mL, 20.0 mmol) and crushed KOH (1.12 g, 20.0 mmol) were added to the solution. Aqueous NH₃ (32%, 38.5 mL) was slowly added to the reaction mixture. This was stirred at room temperature (ca. 22 °C) overnight. The solid that formed was collected by filtration, washed with H₂O (3 × 10 mL) and EtOH (3 × 10 mL), recrystallized from MeOH, and dried in vacuo. Compound 1 was isolated as a colorless solid (1.54 g, 4.00 mmol, 40.0%). M.p. = 218 °C. ¹H NMR (500 MHz, CDCl₃): δ/ppm 9.40 (d, *J* = 2.2 Hz, 2H, H^{A2}), 8.72 (dd, *J* = 4.7, 1.7 Hz, 2H, H^{A6}), 8.53 (dt, *J* = 7.9, 2.2 Hz, 2H, H^{A4}), 8.01 (s, 2H, H^{B3}), 7.85 (d, *J* = 8.4 Hz, 2H, H^{C2}), 7.79 (d, *J* = 8.4 Hz, 2H, H^{C3}), 7.68 (m, 2H, H^{D2}), 7.50 (m, 2H, H^{D3}), 7.47 (m, 2H, H^{A5}), 7.42 (m, 1H, H^{D4}). ¹³C{¹H} NMR (126 MHz, CDCl₃): δ/ppm 155.6 (C^{A3}), 150.6 (C^{B4}), 150.4 (C^{A6}), 148.6 (C^{A2}), 142.6 (C^{C4}), 140.3 (C^{D1}), 137.1 (C^{C1}), 134.8 (C^{B2}), 134.7 (C^{A4}), 129.1 (C^{D3}), 128.2 (C^{C3}), 128.0 (C^{D4}), 127.7 (C^{C2}), 127.3 (C^{D2}), 123.8 (C^{A5}), 117.7 (C^{B3}). UV-VIS (MeCN, 2.0 × 10⁻⁵ mol dm⁻³) λ/nm 228 (ε/dm³ mol⁻¹ cm⁻¹ 28,400), 265 sh (34,600), 284 (41,100). ESI-MS *m/z* 386.13 [M + H]⁺ (calc. 386.17). Found C 83.91, H 4.81, N 11.04; required for C₂₇H₁₉N₃ C 84.13, H 4.97, N 10.90.

2.3. Compound 2

4'-Fluoro-[1,1'-biphenyl]-4-carbaldehyde (2.00 g, 10.0 mmol) was dissolved in EtOH (50 mL). 3-Acetylpyridine (2.42 g, 2.20 mL, 20.0 mmol) and crushed KOH (1.12 g, 20.0 mmol) were added, followed by the slow addition of aqueous NH₃ (32%, 38.5 mL). The reaction mixture was stirred at room temperature overnight, and the solid that formed was collected by filtration, washed with H₂O (3 × 10 mL) and EtOH (3 × 10 mL). The product was recrystallized from MeOH, and dried in vacuo. Compound 2 was isolated as a colorless solid (1.62 g, 4.03 mmol, 40.3%). M.p. = 215 °C. ¹H NMR (500 MHz, CDCl₃): δ/ppm 9.39 (d, *J* = 2.2 Hz, 2H, H^{A2}), 8.71 (dd, *J* = 4.7, 1.5 Hz, 2H, H^{A6}), 8.53 (dt, *J* = 8.0, 2.2 Hz, 2H, H^{A4}), 8.00 (s, 2H, H^{B3}), 7.84 (m, 2H, H^{C2}), 7.74 (m, 2H, H^{C3}), 7.63 (m, 2H, H^{D2}), 7.48 (ddd, *J* = 8.0, 4.7, 0.9 Hz, 2H, H^{A5}), 7.18 (m, 2H, H^{D3}). ¹³C{¹H} NMR (126 MHz, CDCl₃): δ/ppm 162.9 (d, *J*_{CF} = 239 Hz, C^{D4}), 155.6 (C^{A3}), 150.5 (C^{B4}), 150.3 (C^{A6}), 148.5 (C^{A2}), 141.6 (C^{C4}), 137.1 (C^{C1}), 136.4 (d, *J*_{CF} = 2.5 Hz, C^{D1}), 134.85 (C^{B2}), 134.8 (C^{A4}), 128.9 (d, *J*_{CF} = 7.6 Hz, C^{D2}), 128.0 (C^{C3}), 127.8 (C^{C2}), 123.8 (C^{A5}), 117.7 (C^{B3}), 116.1 (d, *J*_{CF} = 22.5 Hz, C^{D3}). ¹⁹F{¹H} NMR (470 MHz, CDCl₃): δ/ppm -114.6. UV-VIS (MeCN, 2.0 × 10⁻⁵ mol dm⁻³) λ/nm 227 (ε/dm³ mol⁻¹ cm⁻¹ 28,200), 264 sh (33,100), 284 (38,800). ESI-MS *m/z* 404.12 [M + H]⁺ (calc. 404.16). Found C 79.08, H 4.59, N 10.42; required for C₂₇H₁₈FN₃ C 80.38, H 4.50, N 10.42.

2.4. Compound 3

4'-Chloro-[1,1'-biphenyl]-4-carbaldehyde (2.17 g, 10.0 mmol) was dissolved in EtOH (50 mL), and then 3-acetylpyridine (2.42 g, 2.20 mL, 20.0 mmol) and crushed KOH (1.12 g, 20.0 mmol) were added to the solution. Aqueous NH₃ (32%, 38.5 mL) was slowly added to the reaction mixture, which was then stirred at room temperature overnight. The solid that formed was collected by filtration, washed with H₂O (3 × 10 mL) and EtOH (3 × 10 mL), recrystallized from EtOH, and dried in vacuo. Compound 3 was isolated as a colorless solid (1.43 g, 3.40 mmol, 34.0%). M.p. = 240 °C. ¹H NMR (500 MHz, CDCl₃): δ/ppm 9.40 (dd, *J* = 2.2, 0.9 Hz, 2H, H^{A2}), 8.72 (dd, *J* = 4.8, 1.6 Hz, 2H, H^{A6}), 8.54 (dt, *J* = 8.1, 2.2 Hz, 2H, H^{A4}), 8.00 (s, 2H, H^{B3}), 7.84 (m, 2H, H^{C2}), 7.75 (m, 2H, H^{C3}), 7.60 (m, 2H, H^{D2}), 7.50–7.44 (overlapping m, 4H, H^{A5+D3}). ¹³C{¹H} NMR (126 MHz, CDCl₃): δ/ppm 155.6 (C^{A3}), 150.4 (C^{B4}), 150.3 (C^{A6}), 148.5 (C^{A2}), 141.3 (C^{C4}), 138.7 (C^{D4}), 137.5 (C^{C1}), 134.84 (C^{B2}), 134.8 (C^{A4}), 134.2 (C^{D1}), 129.3 (C^{D3}), 128.5 (C^{D2}), 128.0 (C^{C3}), 127.8 (C^{C2}), 123.8 (C^{A5}), 117.7 (C^{B3}). UV-VIS (MeCN, 2.0 × 10⁻⁵ mol dm⁻³) λ/nm 228 (ε/dm³ mol⁻¹ cm⁻¹ 29,000), 264 sh (35,800), 288 (45,900). ESI-MS *m/z* 420.09 [M + H]⁺ (calc. 420.13). Found C 76.58, H 4.12, N 9.87; required for C₂₇H₁₈ClN₃ C 77.23, H 4.32, N 10.01.

2.5. Compound 4

4'-Bromo-[1,1'-biphenyl]-4-carboxaldehyde (0.809 g, 3.1 mmol) was dissolved in EtOH (50 mL), then 3-acetylpyridine (0.751 g, 0.683 mL, 6.2 mmol) and crushed KOH (0.348 g, 6.2 mmol) were added. Aqueous NH₃ (32%, 11.9 mL) was slowly added to the reaction mixture, and this was stirred at room temperature overnight. The solid product was collected by filtration, washed with H₂O (3 × 10 mL) and EtOH (3 × 10 mL), and dried in vacuo. Compound 4 was isolated as a colorless solid (0.645 g, 1.39 mmol, 44.8%). M.p. = 248 °C. ¹H NMR (500 MHz, CDCl₃): δ/ppm 9.40 (dd, *J* = 2.3, 0.9 Hz, 2H, H^{A2}), 8.72 (dd, *J* = 4.8, 1.7 Hz, 2H, H^{A6}), 8.54 (dt, *J* = 8.0, 2.3 Hz, 2H, H^{A4}), 8.00 (s, 2H, H^{B3}), 7.84 (m, 2H, H^{C2}), 7.75 (m, 2H, H^{C3}), 7.62 (m, 2H, H^{D3}), 7.54 (m, 2H, H^{D2}), 7.44 (m, 2H, H^{A5}). ¹³C{¹H} NMR (126 MHz, CDCl₃): δ/ppm 155.6 (C^{A3}), 150.4 (C^{B4}), 150.3 (C^{A6}), 148.5 (C^{A2}), 141.3 (C^{C4}), 139.2 (C^{D1}), 137.5 (C^{C1}), 134.83 (C^{B2}), 134.81 (C^{A4}), 132.3 (C^{D3}), 128.9 (C^{D2}), 128.0 (C^{C3}), 127.9 (C^{C2}), 123.9 (C^{A5}), 122.4 (C^{D4}), 117.7 (C^{B3}). UV-VIS (MeCN, 2.0 × 10⁻⁵ mol dm⁻³) λ/nm 228 (ε/dm³ mol⁻¹ cm⁻¹ 29,000), 264 sh (35,800), 292 (47,000). ESI-MS *m/z* 464.05 [M + H]⁺ (calc. 464.08). Found C 69.55, H 3.76, N 8.89; required for C₂₇H₁₈ BrN₃ C 69.84, H 3.91, N 9.05.

2.6. Compound 5

4'-Methyl-[1,1'-biphenyl]-4-carbaldehyde (1.00 g, 5.09 mmol) was dissolved in EtOH (50 mL), and 3-acetylpyridine (1.23 g, 1.12 mL, 10.2 mmol) was added, followed by crushed KOH (0.571 g, 10.2 mmol). Aqueous NH₃ (32%, 19.6 mL) was added slowly to the reaction mixture, which was then stirred at room temperature overnight. The solid product was collected by filtration, washed with H₂O (3 × 10 mL) and EtOH (3 × 10 mL), recrystallized from EtOH, and dried in vacuo. Compound 5 was isolated as a colorless solid (0.670 g, 1.68 mmol, 32.9%). M.p. = 191 °C. ¹H NMR (500 MHz, CDCl₃): δ/ppm 9.40 (d, *J* = 0.9 Hz, 2H, H^{A2}), 8.72 (dd, *J* = 4.8, 1.7 Hz, 2H, H^{A6}), 8.53 (dt, *J* = 8.0, 2.0 Hz, 2H, H^{A4}), 8.01 (s, 2H, H^{B3}), 7.83 (d, *J* = 8.2 Hz, 2H, H^{C2}), 7.78 (d, *J* = 8.2 Hz, 2H, H^{C3}), 7.58 (d, *J* = 8.0 Hz, 2H, H^{D2}), 7.48 (m, 2H, H^{A5}), 7.31 (d, *J* = 8.0 Hz, 2H, H^{D3}), 2.43 (s, 3H, H^{Me}). ¹³C{¹H} NMR (126 MHz, CDCl₃): δ/ppm 155.6 (C^{A3}), 150.7 (C^{B4}), 150.3 (C^{A6}), 148.5 (C^{A2}), 142.5 (C^{C4}), 138.0 (C^{D4}), 137.3 (C^{D1}), 136.8 (C^{C1}), 134.9 (C^{B2}), 134.8 (C^{A4}), 129.8 (C^{D3}), 127.9 (C^{C3}), 127.7 (C^{C2}), 127.1 (C^{D2}), 123.8 (C^{A5}), 117.7 (C^{B3}), 21.3 (C^{Me}). UV-VIS (MeCN, 2.0 × 10⁻⁵ mol dm⁻³) λ/nm 230 (ε/dm³ mol⁻¹ cm⁻¹ 30,500), 261 sh (31,100), 295 (38,000). ESI-MS *m/z* 400.16 [M + H]⁺ (calc. 400.18). Found C 83.89, H 5.30, N 10.39; required for C₂₈H₂₁N₃ C 84.18, H 5.30, N 10.52.

2.7. Crystal Growth of [Cu₂(μ-OAc)₄(1)]_n and Preparative Scale Reaction

A solution of Cu₂(OAc)₄·2H₂O (12.0 mg, 0.030 mmol) in MeOH (5 mL) was layered over a CHCl₃ solution (4 mL) of **1** (11.6 mg, 0.030 mmol). Blue block-like crystals grew after 11 days. A single crystal was selected for X-ray diffraction, and the remaining crystals were washed with MeOH and CHCl₃, dried under vacuum, and analyzed by powder X-ray diffraction (PXRD) and FT-IR spectroscopy.

A blue solution of Cu₂(OAc)₄·2H₂O (79.9 mg, 0.200 mmol) in MeOH (30 mL) was added to a colorless CHCl₃ solution (10 mL) of **1** (77.1 mg, 0.200 mmol) in a round-bottomed flask. The blue solution was stirred at room temperature and after 1 h, a fine light-green suspension had formed. After 2 h, the suspension was centrifuged, and the solid was collected and dried in vacuo until it was a constant weight (6 h). [Cu₂(μ-OAc)₄(1)]_n (24 mg, 0.032 mmol, 16%) was isolated as a light green powder. Found C 56.11, H 4.17, N 5.28; required for C₃₅H₃₁Cu₂N₃O₈: C 56.15, H 4.17, N 5.61. PXRD analysis was performed (see text).

2.8. Crystal Growth of [Cu₂(μ-OAc)₄(2)]_n and Preparative Scale Reaction

A solution of Cu₂(OAc)₄·2H₂O (12.0 mg, 0.030 mmol) in MeOH (5 mL) was layered over a CHCl₃ solution (4 mL) of **2** (12.1 mg, 0.030 mmol), and after 20 days, blue blocks of X-ray quality had grown. A single crystal was selected for X-ray diffraction, and the rest of

the crystals were washed with MeOH and CHCl₃, dried in vacuo, and were analyzed by PXRD and FT-IR spectroscopy.

A blue solution of Cu₂(OAc)₄·2H₂O (79.9 mg, 0.200 mmol) in MeOH (30 mL) was added to a colorless CHCl₃ solution (15 mL) of **2** (80.7 mg, 0.200 mmol) in a round-bottomed flask. The blue solution was stirred at room temperature, and after 1 h, a fine light green suspension had formed. After 2 h, the solid was collected using a centrifuge and was dried in vacuo until a constant weight was achieved (6 h). [Cu₂(μ-OAc)₄(**2**)_n] (101 mg, 0.132 mmol, 66.0%) was isolated as a light-green solid. Found C 54.43, H 3.86, N 5.43; required for C₃₅H₃₀Cu₂FN₃O₈: C 54.83, H 3.94, N 5.48. See text for PXRD.

2.9. Crystal Growth of [Cu₂(μ-OAc)₄(**3**)_n] and Preparative Scale Reaction

A MeOH (4 mL) solution of Cu₂(OAc)₄·2H₂O (12.0 mg, 0.030 mmol) was layered over a CHCl₃ solution (4 mL) of **3** (12.6 mg, 0.030 mmol). After eight days, X-ray quality green plate-like crystals had grown. One crystal was selected for single-crystal X-ray diffraction, and the remaining crystals were washed with MeOH and CHCl₃, dried under vacuum, and analyzed by PXRD and FT-IR spectroscopy.

A solution of Cu₂(OAc)₄·2H₂O (79.9 mg, 0.200 mmol) in MeOH (30 mL) was added to a solution of **3** (84.0 mg, 0.200 mmol) in CHCl₃ (15 mL) in a round-bottomed flask. The blue solution was stirred at room temperature, and after about 5 min, a fine light green suspension had formed. After 2 h, the suspension was centrifuged, and the solid was dried in vacuo until it was a constant weight (6 h). [Cu₂(μ-OAc)₄(**3**)_n] (126 mg, 0.161 mmol, 80.5%) was isolated as a light green powder. Found C 53.13, H 3.74, N 5.30; required for C₃₅H₃₀Cu₂ClN₃O₈: C 53.68, H 3.86, N 5.37. See text for PXRD.

2.10. Crystal Growth of [Cu₂(μ-OAc)₄(**4**)_n] and Preparative Scale Reaction

Cu₂(OAc)₄·2H₂O (12.0 mg, 0.030 mmol) was dissolved in MeOH (4 mL), and the solution was layered over a CHCl₃ solution (4 mL) of **4** (13.9 mg, 0.030 mmol). Green plate-like crystals had grown after 20 days, and a single crystal was selected for X-ray diffraction. The remaining crystals were washed with MeOH and CHCl₃, dried under vacuum, and analyzed by PXRD and FT-IR spectroscopy.

A solution of Cu₂(OAc)₄·2H₂O (79.9 mg, 0.200 mmol) in MeOH (30 mL) was added to a CHCl₃ solution (15 mL) of **4** (92.9 mg, 0.200 mmol) in a round-bottomed flask. The blue solution was stirred at room temperature, and a light-green suspension was observed after about 5 min. After 2 h, the suspension was centrifuged, and the solid was dried in vacuo to a constant weight (6 h). [Cu₂(μ-OAc)₄(**4**)_n] (132 mg, 0.0797 mmol, 79.7%) was isolated as a light green powder. Found C 49.87, H 3.51, N 4.94; required for C₇₀H₆₀Cu₄Br₂N₆O₁₆: C 50.79, H 3.65, N 5.08. See text for PXRD.

2.11. Crystal Growth of [Cu₂(μ-OAc)₄(**5**)_n]·nMeOH and Preparative Scale Reaction

Cu₂(OAc)₄·2H₂O (12.0 mg, 0.030 mmol) was dissolved in MeOH (4 mL), and the solution was layered over a CHCl₃ solution (4 mL) of **5** (11.9 mg, 0.030 mmol). After 25 days, X-ray quality green plates had grown, and a single crystal was selected for X-ray diffraction. The rest of the crystals were washed with MeOH and CHCl₃, dried in vacuo, and analyzed by PXRD and FT-IR spectroscopy.

A solution of Cu₂(OAc)₄·2H₂O (79.9 mg, 0.200 mmol) in MeOH (30 mL) was added to a CHCl₃ solution (10 mL) of **5** (79.9 mg, 0.200 mmol) in a round-bottomed flask. The blue solution was stirred at room temperature, and a light-green suspension was observed after about 10 min. After 2 h, the suspension was centrifuged, and the solid was dried under vacuum until the weight was constant (6 h). [Cu₂(μ-OAc)₄(**5**)_n] (108 mg, 0.0708 mmol, 70.8%) was isolated as a light green powder. Found C 56.30, H 4.27, N 5.50; required for C₇₂H₆₆Cu₄N₆O₁₆: C 56.69, H 4.36, N 5.51. See text for PXRD.

2.12. Crystallography

Single crystal data were collected on a Bruker APEX-II diffractometer (CuK α radiation) with data reduction, solution, and refinement using the programs APEX [30], ShelXT [31], Olex2 [32], and ShelXL v. 2014/7 [33], or using a STOE StadiVari diffractometer equipped with a Pilatus300K detector and with a Metaljet D2 source (GaK α radiation) and solving the structure using Superflip [34,35] and Olex2 [32]. See Sections 2.13–2.17 for the radiation type (Cu or Ga). The model was refined with ShelXL v. 2014/7 [33]. Structure analysis including the ORTEP-type representations used CSD Mercury 2020.1 [36]. In [Cu₂(μ -OAc)₄(5)]_n·*n*MeOH, the MeOH solvent molecule was disordered over two orientations and was modelled with 75% and 25% occupancy of the sites.

Powder X-Ray diffraction (PXRD) patterns were collected at room temperature in transmission mode using a Stoe Stadi P diffractometer equipped with a Cu K α 1 radiation (Ge(111) monochromator) and a DECTRIS MYTHEN 1K detector. Whole-pattern decomposition (profile matching) analysis [37–39] of the diffraction patterns was performed with the package FULLPROF SUITE [39,40] (version July-2019) using a previously determined instrument resolution function based on a NIST640d standard. The structural models were taken from the single crystal X-Ray diffraction refinements. Refined parameters in Rietveld were scale factor, zero shift, lattice parameters, Cu and halogen atomic positions, background points, and peaks shapes as a Thompson–Cox–Hastings pseudo-Voigt function. Preferred orientations as a March–Dollase multi-axial phenomenological model were incorporated into the analysis.

2.13. [Cu₂(μ -OAc)₄(1)]_n

C₃₅H₃₁Cu₂N₃O₈, *M_r* = 748.71, blue block, monoclinic, space group *C2/c*, *a* = 27.7823(14), *b* = 15.4445(11), *c* = 7.9423(4) Å, β = 102.301(4)°, *V* = 3329.7(3) Å³, *D_c* = 1.494 g cm⁻³, *T* = 150 K, *Z* = 4, μ (GaK α) = 7.203 mm⁻¹. Total 20,589 reflections, 3485 unique (*R_{int}* = 0.0693). Refinement of 2756 reflections (222 parameters) with *I* > 2 σ (*I*) converged at final *R*₁ = 0.0656 (*R*₁ all data = 0.0979), *wR*₂ = 0.1287 (*wR*₂ all data = 0.1526), *gof* = 1.212. CCDC 2042171.

2.14. [Cu₂(μ -OAc)₄(2)]_n

C₃₅H₃₀Cu₂FN₃O₈, *M_r* = 766.70, blue block, monoclinic, space group *C2/c*, *a* = 27.6940(16), *b* = 15.9902(7), *c* = 7.8753(6) Å, β = 102.343(5)°, *V* = 3406.8(4) Å³, *D_c* = 1.495 g cm⁻³, *T* = 150 K, *Z* = 4, μ (GaK α) = 7.077 mm⁻¹. Total 26,608 reflections, 3531 unique (*R_{int}* = 0.0845). Refinement of 2854 reflections (227 parameters) with *I* > 2 σ (*I*) converged at final *R*₁ = 0.0907 (*R*₁ all data = 0.1116), *wR*₂ = 0.2310 (*wR*₂ all data = 0.2590), *gof* = 1.151. CCDC 2042172.

2.15. [Cu₂(μ -OAc)₄(3)]_n

C₃₅H₃₀Cu₂ClN₃O₈, *M_r* = 783.15, green plate, triclinic, space group *P*-1, *a* = 8.0001(3), *b* = 9.3586(3), *c* = 23.7240(7) Å, α = 99.3320(10), β = 96.370(2), γ = 98.442(2), *V* = 1717.11(10) Å³, *D_c* = 1.515 g cm⁻³, *T* = 150 K, *Z* = 2, *Z'* = 1, μ (CuK α) = 2.714 mm⁻¹. Total 20,409 reflections, 6355 unique (*R_{int}* = 0.0293). Refinement of 5729 reflections (446 parameters) with *I* > 2 σ (*I*) converged at final *R*₁ = 0.0457 (*R*₁ all data = 0.0502), *wR*₂ = 0.1286 (*wR*₂ all data = 0.1340), *gof* = 1.054. CCDC 2042175.

2.16. [Cu₂(μ -OAc)₄(4)]_n

C₇₀H₆₀Cu₄Br₂N₆O₁₆, *M_r* = 1655.22, green plate, triclinic, space group *P*-1, *a* = 7.9898(5), *b* = 9.3656(5), *c* = 23.6072(13) Å, α = 98.626(2), β = 96.301(2), γ = 97.555(2)°, *V* = 1716.19(17) Å³, *D_c* = 1.602 g cm⁻³, *T* = 150 K, *Z* = 1, μ (CuK α) = 3.363 mm⁻¹. Total 27,701 reflections, 6338 unique (*R_{int}* = 0.0236). Refinement of 6120 reflections (446 parameters) with *I* > 2 σ (*I*) converged at final *R*₁ = 0.0482 (*R*₁ all data = 0.0493), *wR*₂ = 0.1317 (*wR*₂ all data = 0.1328), *gof* = 1.072. CCDC 2042174.

2.17. $[Cu_2(\mu-OAc)_4(5)]_n \cdot nMeOH$

$C_{74}H_{74}Cu_4N_6O_{18}$, $M_r = 1589.55$, green plate, triclinic, space group $P\bar{1}$, $a = 8.0240(4)$, $b = 9.4295(5)$, $c = 23.8856(11)$ Å, $\alpha = 100.7670(10)$, $\beta = 95.673(2)$, $\gamma = 97.244(2)^\circ$, $V = 1747.30(15)$ Å³, $D_c = 1.511$ g cm⁻³, $T = 150$ K, $Z = 1$, $\mu(CuK\alpha) = 2.008$ mm⁻¹. Total 21,488 reflections, 6397 unique ($R_{int} = 0.0280$). Refinement of 6197 reflections (477 parameters) with $I > 2\sigma(I)$ converged at final $R_1 = 0.0366$ (R_1 all data = 0.0374), $wR_2 = 0.1030$ (wR_2 all data = 0.1038), $gof = 1.053$. CCDC 2042173.

2.18. Density Functional Theory (DFT) Calculations

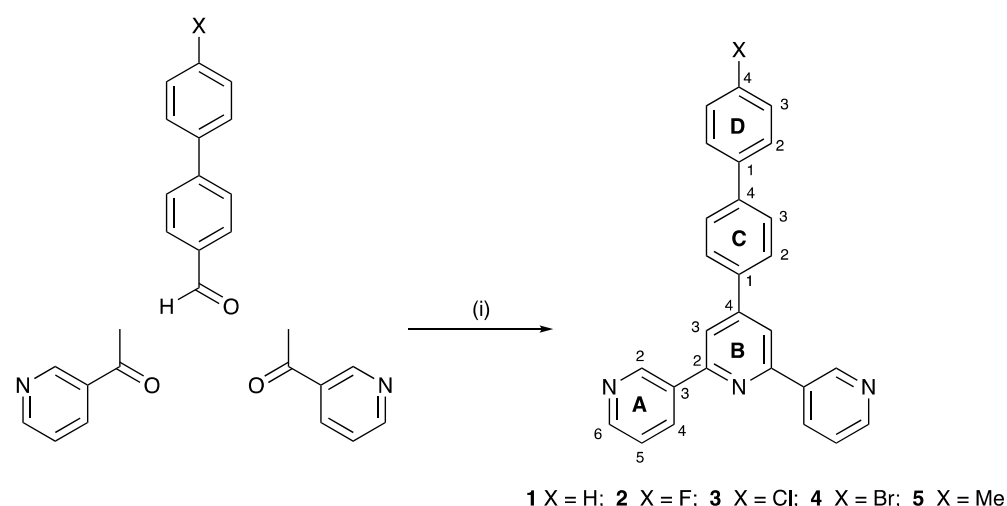
DFT calculations on ligands 2–4 were carried out using Spartan'18 [41] with a B3LYP 6-31G* basis set with geometry optimization first carried out at the semi-empirical PM3 level.

3. Results and Discussion

3.1. Ligand Synthesis and Characterization

Compounds 1–5 were prepared using the one-pot method of Hanan [10] as shown in Scheme 5. The products precipitated from the reaction mixtures and were isolated in yields varying from 32.9% (for 5) to 44.8% (for 4). No attempts were made to optimize the reaction conditions. In the electrospray mass spectrum of each compound, the base peak arose from the $[M + H]^+$ ion (Figures S1–S5 in the Supporting Material) with characteristic isotope patterns observed for compounds 3 (chloro derivative) and 4 (bromo substituent).

The ¹H and ¹³C{¹H} NMR spectra of compounds 1–5 were assigned with the aid of COSY, NOESY, HMQC, and HMBC techniques, and ¹H NMR, NOESY, HMQC, and HMBC spectra are shown in Figures S6–S25 in the Supporting Material. Figure 1 displays a comparison of the ¹H NMR spectra of 1–5. The signals arising from the protons in rings A, B, and C (see Scheme 5 for ring labels) are unaffected by the change in the substituent in ring D. Assignments of the signals for H^{D2} and H^{D3} (Figure 1) were confirmed from the NOESY cross peaks between H^{C3} and H^{D2}, protons H^{C2} and H^{C3} being first distinguished using the NOESY H^{B3}/H^{C2} crosspeaks (compare Figures S7, S11, S15, S19 and S23). The change from X = H in 1 (Scheme 5) to the halogen substituents in 2, 3, and 4 and Me group in 5 has the most significant effect on H^{D3}, consistent with expectations [42]. The IR spectra of the new ligands are shown in Figures S26–S30.



Scheme 5. Synthetic route to compounds 1–5. Conditions: (i) KOH, EtOH; NH₃ (aqueous), room temperature, ca. 15 h. Atom numbering for the NMR spectroscopic assignments is given.

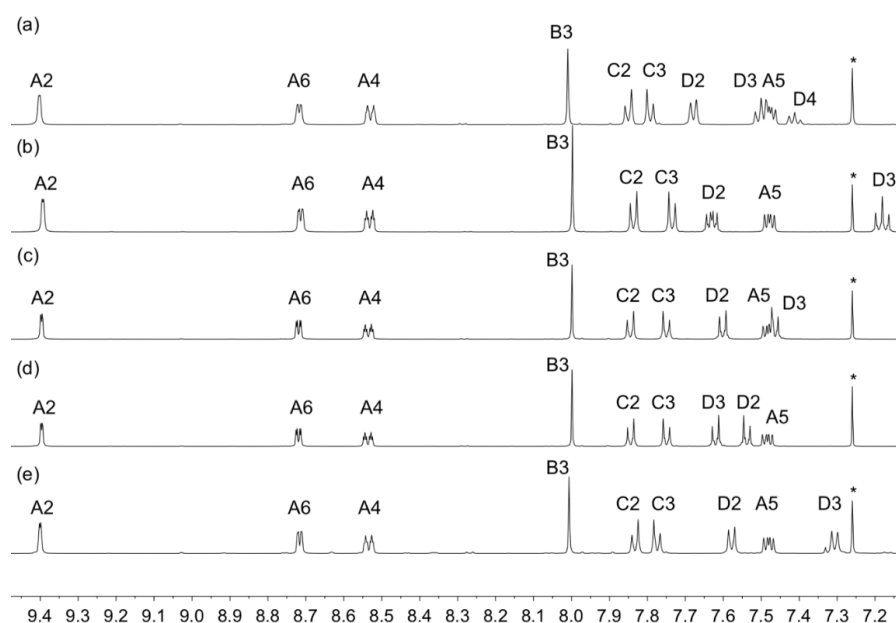


Figure 1. ^1H NMR spectra (aromatic region) for compounds (a) **1**, (b) **2**, (c) **3**, (d) **4** and (e) **5** (500 MHz, CDCl_3 , 298 K). * = residual CHCl_3 .

The absorption spectra of acetonitrile solutions of compounds **1–5** are shown in Figure 2a. Each spectrum is dominated by a broad and intense band arising principally from $\pi^* \leftarrow \pi$ transitions. For the three halogen-substituted compounds, the value of λ_{max} shifts from 284 nm (F) to 288 nm (Cl) to 292 nm (Br), consistent with a stabilization of the highest-occupied molecular orbital(s) for the more electron-withdrawing substituent. DFT calculations on ligands **2**, **3**, and **4** revealed that the highest occupied molecular orbital (HOMO) of each complex is localized on the 4'-halo-[1,1'-biphenyl] domain, while the lowest unoccupied molecular orbital (LUMO) manifold is largely localized on the 3,2':6',3''-tpy unit (Figure 2b). The HOMO–1 is, in each case, localized on the 3,2':6',3''-tpy.

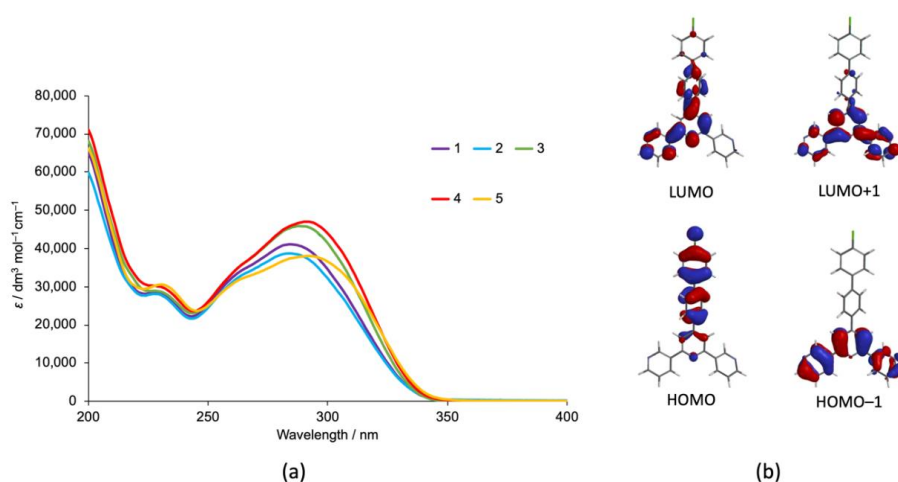


Figure 2. (a) Solution absorption spectra (MeCN , $2.0 \times 10^{-5} \text{ mol dm}^{-3}$) of compounds **1–5**. (b) Highest occupied and lowest unoccupied molecular orbital compositions in compound **3**; similar compositions are seen in **2** and **4**.

3.2. Reactions of Copper(II) Acetate and Ligands **1–5**

Ligands **1–5** were allowed to react with copper(II) acetate under ambient conditions by layering a methanol solution of $\text{Cu}_2(\text{OAc})_4 \cdot 2\text{H}_2\text{O}$ over a chloroform solution of the appropriate ligand. Single crystals grew within days or several weeks, and after selection

of crystals for single crystal X-ray analysis, the remaining crystals were washed with MeOH and CHCl_3 , dried, and analyzed by PXRD to confirm that the single crystals were representative of the bulk sample (see Section 3.4). The solid-state IR spectra of the bulk materials are all similar and are presented in Figures S31–S35 in the Supporting Material. Yields of the products from the single-crystal growth experiments were not optimized, and were in the range 20–30% if crystal growth was allowed to continue for a month.

The reactions were also carried out on a preparative scale by combining a methanol solution of $\text{Cu}_2(\text{OAc})_4 \cdot 2\text{H}_2\text{O}$ with a chloroform solution of the respective ligand. The precipitate that formed was separated by centrifugation, dried, and analyzed by elemental analysis and PXRD. Elemental analytical data were in accord with the compositions $[\text{Cu}_2(\mu\text{-OAc})_4(\text{L})]_n$ with $\text{L} = 1\text{--}5$. The PXRD data are discussed in Section 3.4.

3.3. Single Crystal Structures

The single-crystal structures of the five copper(II) complexes confirmed the assembly of one-dimensional coordination polymers containing the ubiquitous $\{\text{Cu}_2(\text{OAc})_4\}$ paddlewheel motif. The polymers $[\text{Cu}_2(\mu\text{-OAc})_4(\mathbf{1})]_n$ and $[\text{Cu}_2(\mu\text{-OAc})_4(\mathbf{2})]_n$ crystallize in the monoclinic space group $C2/c$ with similar cell dimensions (see Sections 2.13 and 2.14). In contrast, the $[\text{Cu}_2(\mu\text{-OAc})_4(\mathbf{3})]_n$, $[\text{Cu}_2(\mu\text{-OAc})_4(\mathbf{4})]_n$, and $[\text{Cu}_2(\mu\text{-OAc})_4(\mathbf{5})]_n \cdot n\text{MeOH}$ crystallize in the triclinic space group $P-1$, again with similar cell dimensions for the series of compounds. Only the coordination compound containing ligand **5** contains lattice solvent. ORTEP-type diagrams of the repeating units in each coordination polymer are displayed in Figures 3 and 4, and selected bond lengths are given in Table 1. The bond parameters for the $\{\text{Cu}_2(\mu\text{-OAc})_4\}$ units are unexceptional, and the Cu–N bond distances are typical with the exception of Cu1–N1 in $[\text{Cu}_2(\mu\text{-OAc})_4(\mathbf{5})]_n \cdot n\text{MeOH}$. This bond is somewhat elongated (2.1813(19) Å), and this appears to be associated with the presence of a MeOH molecule, which is hydrogen-bonded to one acetato bridge (Figure 5) and resides in a pocket close to one Cu–N bond. The five coordination polymers fall into two structural classes, which differ in the conformation of the 3,2':6',3''-tpy unit. In $[\text{Cu}_2(\mu\text{-OAc})_4(\mathbf{1})]_n$ and $[\text{Cu}_2(\mu\text{-OAc})_4(\mathbf{2})]_n$, the asymmetric unit contains half of a ligand molecule **1** or **2**, and the 3,2':6',3''-tpy unit adopts conformation I (Scheme 2). In the compounds containing ligands **3**, **4**, and **5**, the 3,2':6',3''-tpy domain is in conformation II. The angles between the planes of pairs of adjacent aromatic rings are compiled in Table 2, and the data reveal that the 3,2':6',3''-tpy unit is closer to being planar in $[\text{Cu}_2(\mu\text{-OAc})_4(\mathbf{3})]_n$, $[\text{Cu}_2(\mu\text{-OAc})_4(\mathbf{4})]_n$, and $[\text{Cu}_2(\mu\text{-OAc})_4(\mathbf{5})]_n \cdot n\text{MeOH}$ than in $[\text{Cu}_2(\mu\text{-OAc})_4(\mathbf{1})]_n$ and $[\text{Cu}_2(\mu\text{-OAc})_4(\mathbf{2})]_n$. In addition, the angles between the planes of adjacent rings in the central three-arene ring unit are greater in coordinated ligands **1** and **2** than in **3–5**. An inspection of the dominant packing interactions provides an insight into these differences.

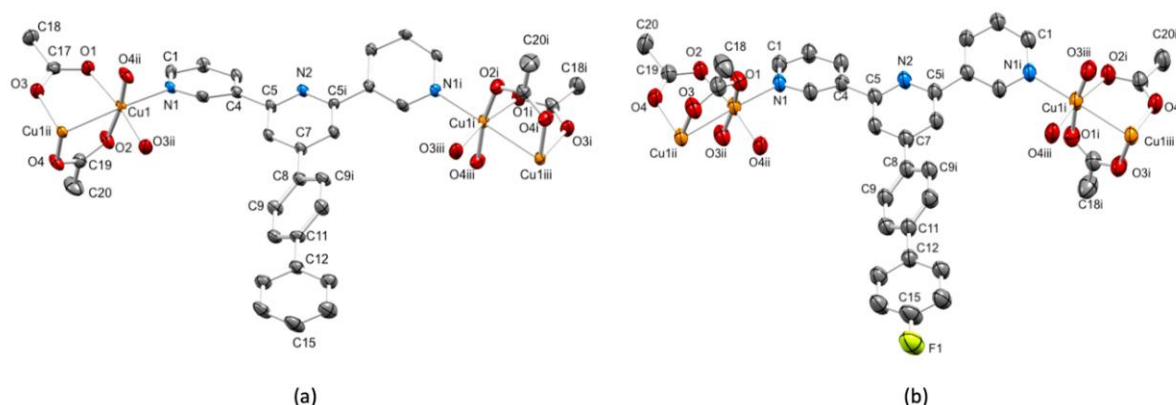


Figure 3. The repeat units (with symmetry generated atoms) in (a) $[\text{Cu}_2(\mu\text{-OAc})_4(\mathbf{2})]_n$ (ellipsoids plotted at 50% probability level; symmetry codes: $i = 1 - x, y, 3/2 - z$; $ii = 3/2 - x, 1/2 - y, 1 - z$; $iii = -1/2 + x, 1/2 - y, 1/2 + z$) and (b) $[\text{Cu}_2(\mu\text{-OAc})_4(\mathbf{1})]_n$ (ellipsoids plotted at 40% probability level; symmetry codes: $i = 1 - x, y, 1/2 - z$; $ii = 1/2 - x, 3/2 - y, 1 - z$; $iii = 1/2 + x, 3/2 - y, -1/2 + z$). H atoms are omitted for clarity.

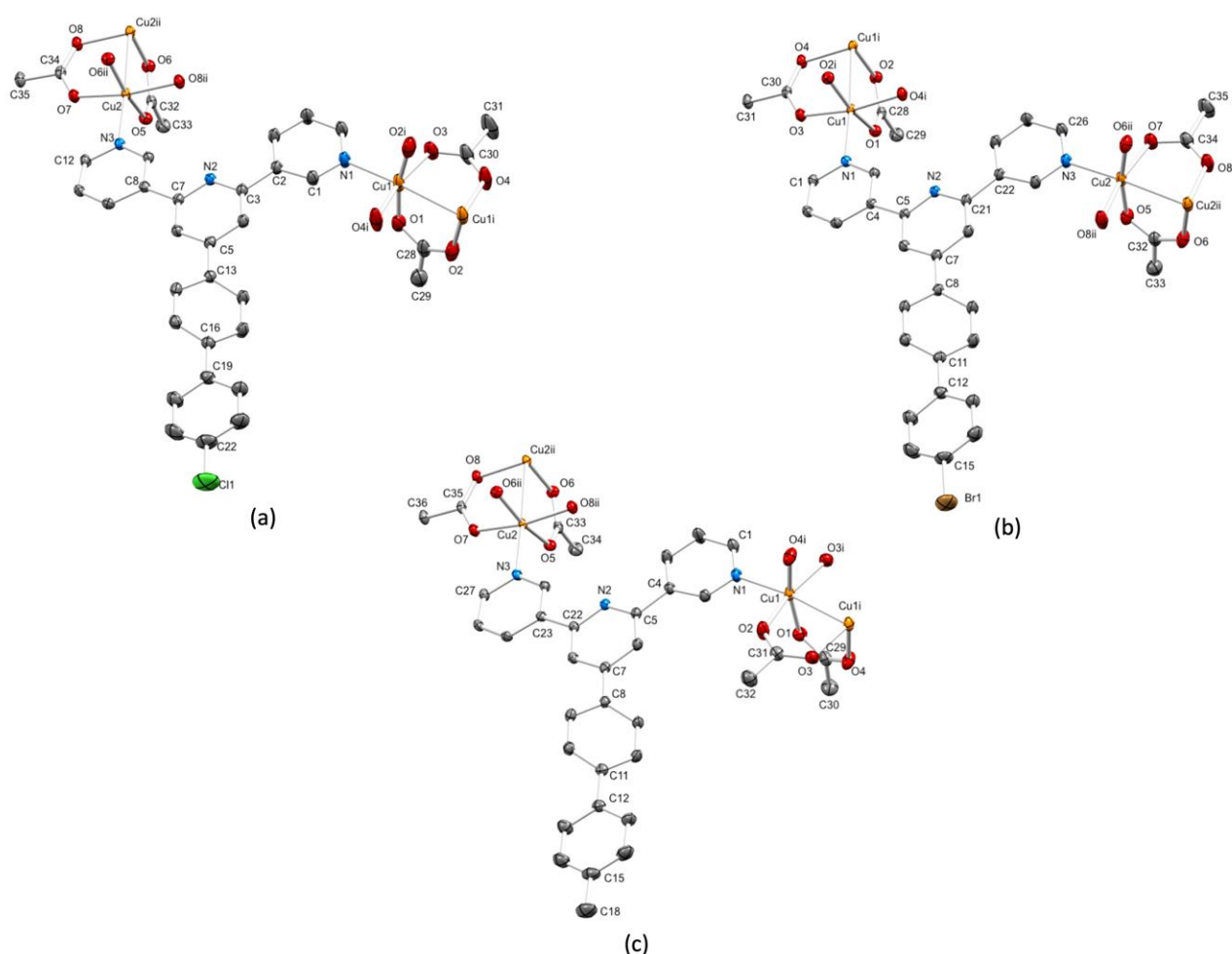


Figure 4. The repeat units (with symmetry generated atoms) in (a) $[\text{Cu}_2(\mu\text{-OAc})_4(\mathbf{3})]_n$ (symmetry codes: $i = 1 - x, 2 - y, 2 - z$; $ii = 2 - x, 2 - y, 1 - z$), (b) $[\text{Cu}_2(\mu\text{-OAc})_4(\mathbf{4})]_n$ (symmetry codes: $i = 2 - x, 2 - y, 1 - z$; $ii = 1 - x, 2 - y, 2 - z$), and (c) $[\text{Cu}_2(\mu\text{-OAc})_4(\mathbf{5})]_n \cdot n\text{MeOH}$ (solvent molecule omitted; symmetry codes: $i = 1 - x, 2 - y, 2 - z$; $ii = 2 - x, 2 - y, 1 - z$). All ellipsoids are plotted at 40% probability level, and H atoms are omitted for clarity.

Table 1. Selected bond lengths in the copper(II) coordination polymers.

| | Cu–O/Å | Cu–N/Å | Cu ... Cu/Å |
|--|---|---------------------------|----------------------|
| $[\text{Cu}_2(\mu\text{-OAc})_4(\mathbf{1})]_n$ | 1.954(4), 1.975(4), 1.990(4), 1.961(4) | 2.157(4) | 2.6051(13) |
| $[\text{Cu}_2(\mu\text{-OAc})_4(\mathbf{2})]_n$ | 1.953(5), 1.994(5), 1.979(5), 1.959(5) | 2.168(5) | 2.6149(17) |
| $[\text{Cu}_2(\mu\text{-OAc})_4(\mathbf{3})]_n$ | 1.9760(18), 1.9894(18), 1.9759(18), 1.9789(18), 1.979(3), 1.970(2), 1.966(3), 1.971(3) | 2.167(2), 2.151(2) | 2.6292(8), 2.6319(7) |
| $[\text{Cu}_2(\mu\text{-OAc})_4(\mathbf{4})]_n$ | 1.973(2), 1.983(2), 1.976(2), 1.979(2), 1.981(3), 1.971(2), 1.972(3), 1.974(3) | 2.153(2), 2.158(3) | 2.6352(8), 2.6235(9) |
| $[\text{Cu}_2(\mu\text{-OAc})_4(\mathbf{5})]_n \cdot n\text{MeOH}$ | 1.9885(15), 1.9787(15), 1.9773(15), 1.9756(15), 1.9887(18), 1.9700(18), 1.9809(19), 1.9644(19) | 2.1510(18), 2.1813(19) | 2.6551(6), 2.6331(6) |

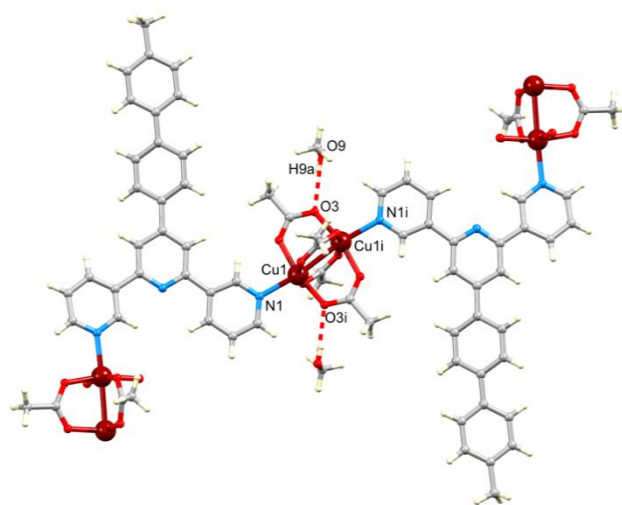


Figure 5. Hydrogen-bonded MeOH molecule in $[\text{Cu}_2(\mu\text{-OAc})_4(\mathbf{5})]_n \cdot n\text{MeOH}$, which resides in a pocket close to the Cu1–N1 bond. Symmetry code: $i = 1 - x, 2 - y, 2 - z$.

Table 2. Angles between ring-planes in the copper(II) coordination polymers.

| | py–py/ $^\circ$ | py _{N2} –Phenylene/ $^\circ$ | Phenylene–phenyl/ $^\circ$ |
|--|-----------------|---------------------------------------|----------------------------|
| $[\text{Cu}_2(\mu\text{-OAc})_4(\mathbf{1})]_n$ | 25.1 | 38.3 | 41.7 |
| $[\text{Cu}_2(\mu\text{-OAc})_4(\mathbf{2})]_n$ | 21.1 | 39.8 | 38.5 |
| $[\text{Cu}_2(\mu\text{-OAc})_4(\mathbf{3})]_n$ | 8.0, 4.5 | 24.0 | 27.2 |
| $[\text{Cu}_2(\mu\text{-OAc})_4(\mathbf{4})]_n$ | 8.1, 4.0 | 22.9 | 26.5 |
| $[\text{Cu}_2(\mu\text{-OAc})_4(\mathbf{5})]_n \cdot n\text{MeOH}$ | 6.5, 4.0 | 27.8 | 28.1 |

In $[\text{Cu}_2(\mu\text{-OAc})_4(\mathbf{1})]_n$ and $[\text{Cu}_2(\mu\text{-OAc})_4(\mathbf{2})]_n$, ligand conformation I leads to a zigzag profile for each 1D-polymer chain, and adjacent chains are arranged with the biphenyl unit directed into the V-shaped cavity of a neighboring 3,2':6',2''-tpy unit (Figure 6). This leads to the assembly of 2D-sheets. Interestingly, the arrangement shown in Figure 6 results in short repulsive H...H contacts in $[\text{Cu}_2(\mu\text{-OAc})_4(\mathbf{1})]_n$, while these are replaced by attractive H...F contacts in $[\text{Cu}_2(\mu\text{-OAc})_4(\mathbf{2})]_n$. This observation suggests that these contacts are not important in supporting the assembly, and this is reminiscent of the isostructural nature of $[\text{Cu}_2(\mu\text{-OAc})_4(\mathbf{6})]_n$ and $[\text{Cu}_2(\mu\text{-OAc})_4(\mathbf{7})]_n$, in which 6 is 4'-([1,1'-biphenyl]-4-yl)-4,2':6',4''-terpyridine and 7 is 4'-(2',3',4',5',6'-pentafluoro [1,1'-biphenyl]-4-yl)-4,2':6',4''-terpyridine [29]. The X...C separations for the X...H–C contacts in the bifurcated interactions in Figure 6 are 3.11 Å for X = H and 3.16 Å for X = F. The dominant packing forces in $[\text{Cu}_2(\mu\text{-OAc})_4(\mathbf{1})]_n$ and $[\text{Cu}_2(\mu\text{-OAc})_4(\mathbf{2})]_n$ are the head-to-tail π -stacking between pairs of [1,1'-biphenyl]pyridine units displayed in Figure 7. Each pair of arene rings adopts an offset arrangement, which is optimal for a π – π interaction [43]. For the pyridine...phenyl interaction in $[\text{Cu}_2(\mu\text{-OAc})_4(\mathbf{1})]_n$, the centroid...centroid distance is 3.97 Å and the angle between the ring planes is 3.4°; the corresponding parameters in $[\text{Cu}_2(\mu\text{-OAc})_4(\mathbf{2})]_n$ are 3.97 Å and 1.4°. For the centrosymmetric pair of phenylene rings, the distances between the ring planes and between their centroids are 3.75 Å and 3.97 Å, respectively, in $[\text{Cu}_2(\mu\text{-OAc})_4(\mathbf{1})]_n$, are 3.71 Å, and 3.96 Å in $[\text{Cu}_2(\mu\text{-OAc})_4(\mathbf{2})]_n$. The cavities in each sheet visible in Figure 7 are occupied by $\{\text{Cu}_2(\mu\text{-OAc})_4\}$ carboxylate groups from an adjacent layer, which protrude above and below each sheet.

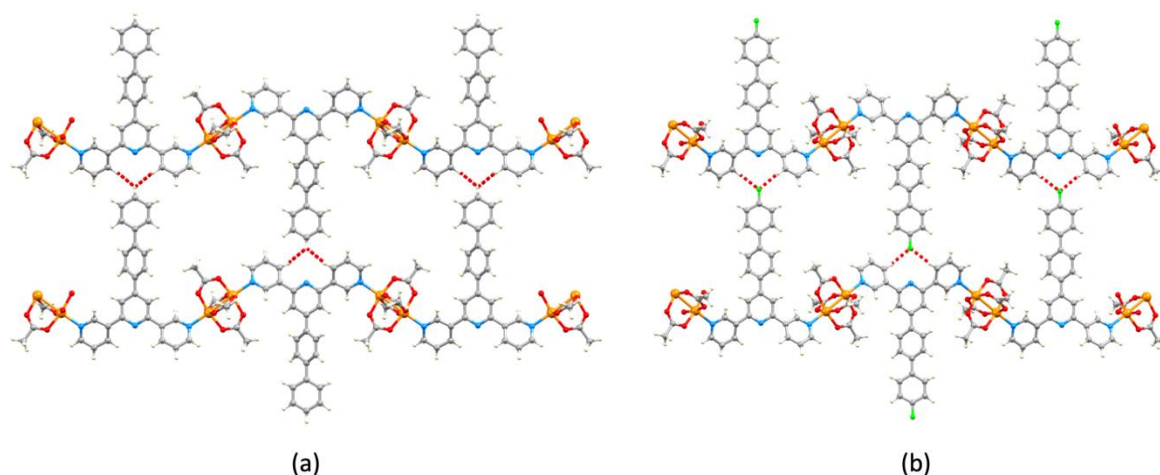


Figure 6. Packing of two adjacent polymer chains in (a) $[\text{Cu}_2(\mu\text{-OAc})_4(1)]_n$ and (b) $[\text{Cu}_2(\mu\text{-OAc})_4(2)]_n$ within one 2D-sheet (see text). The hashed red lines highlight short H...H contacts in $[\text{Cu}_2(\mu\text{-OAc})_4(1)]_n$ and complementary short H...F contacts in $[\text{Cu}_2(\mu\text{-OAc})_4(2)]_n$.

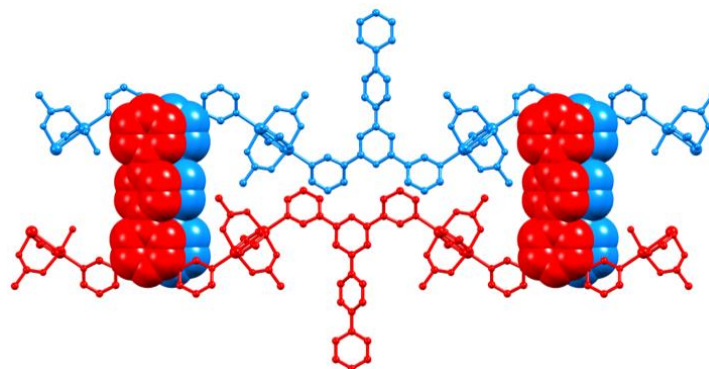


Figure 7. Head-to-tail π -stacking between pairs of [1,1'-biphenyl]pyridine units in adjacent sheets in $[\text{Cu}_2(\mu\text{-OAc})_4(1)]_n$. The same motif is present in $[\text{Cu}_2(\mu\text{-OAc})_4(2)]_n$. H atoms are omitted.

In each of $[\text{Cu}_2(\mu\text{-OAc})_4(3)]_n$, $[\text{Cu}_2(\mu\text{-OAc})_4(4)]_n$, and $[\text{Cu}_2(\mu\text{-OAc})_4(5)]_n \cdot n\text{MeOH}$, the 3,2':6',3''-tpy adopts conformation II (Scheme 2), and the coordination arrangement at the paddle-wheel units (defined in Scheme 3) is *in/in/out/out...* Figure 8a illustrates part of one coordination polymer chain in $[\text{Cu}_2(\mu\text{-OAc})_4(3)]_n$, and this structure is replicated in $[\text{Cu}_2(\mu\text{-OAc})_4(4)]_n$ and $[\text{Cu}_2(\mu\text{-OAc})_4(5)]_n \cdot n\text{MeOH}$, as are the packing motifs described below. Figure 8b illustrates the interdigitation of 1D-polymer chains to produce 2D-sheets. The profile of the chain in Figure 8a contrasts with the zigzag nature of the polymers in Figure 7, and packing interactions are necessarily different. The near planarity of the 3,2':6',3''-tpy unit (Table 2) reflects the involvement of this domain in crystal packing. Centrosymmetric pairs of pyridine rings containing N3 (N3 and N3ⁱⁱⁱ, symmetry code iii = 1 - x, 1 - y, 1 - z) stack with an interplane distance of 3.34 Å and inter-centroid separation of 3.68 Å. The pyridine ring with N1 engages in a face-to-face contact with the phenyl ring containing C22^{iv} (symmetry code iv = 1 + x, 1 + y, z) with a centroid...centroid distance of 3.94 Å and an angle between the ring planes of 11.1°. In addition, the pyridine ring containing N1 also sits over a biphenyl unit, thereby extending the stack of arene rings. The projection shown in Figure 8c illustrates how the layers comprise domains of π -stacked arene rings and columns of $\{\text{Cu}_2(\mu\text{-OAc})_4\}$ paddle-wheel units (see also Figure S36 in the Supporting Material).

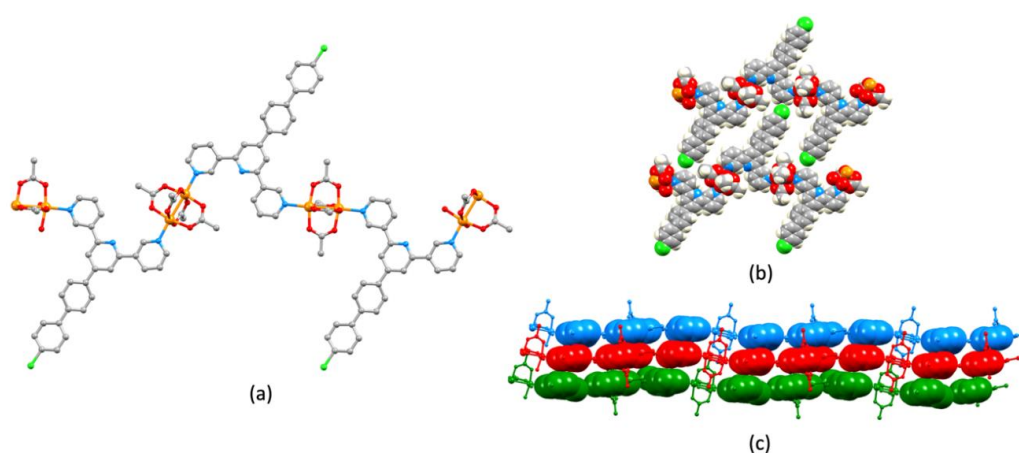


Figure 8. (a) Part of one polymer chain in $[\text{Cu}_2(\mu\text{-OAc})_4(\mathbf{3})]_n$, (b) interdigitation of chains generates a 2D-sheet, and (c) stacking of three adjacent sheets involves both pyridine and biphenyl rings.

3.4. Characterization by PXRD

To ensure that the single crystal structures were representative of the bulk materials, powder X-ray diffraction patterns were determined for crystals remaining in the crystallization tubes after single crystals had been selected. The refinements (Figures S37–S41) confirmed that the bulk materials of all the compounds were representative of the analyzed single crystals. Each peak in the experimental plots has a corresponding peak in the fitted spectra, and the differences in the intensities can be rationalized in terms of differences in the preferred orientations. Only $[\text{Cu}_2(\mu\text{-OAc})_4(\mathbf{2})]_n$ (Figure S38) shows minor impurities (ca. 10%). A comparison of Figure S38 with PXRD patterns for the precursors **2** and $\text{Cu}_2(\text{OAc})_4 \cdot 2\text{H}_2\text{O}$ did not reveal matching peaks.

PXRD was also carried out on the materials obtained from the preparative scale reactions. The powder patterns matched those of the materials obtained from the single-crystal growth experiments. Figure 9 displays the data for $[\text{Cu}_2(\mu\text{-OAc})_4(\mathbf{1})]_n$ as a representative example, and the superimpositions of the powder patterns for the remaining four coordination polymers are shown in Figures S42–S45 in the Supporting Materials.

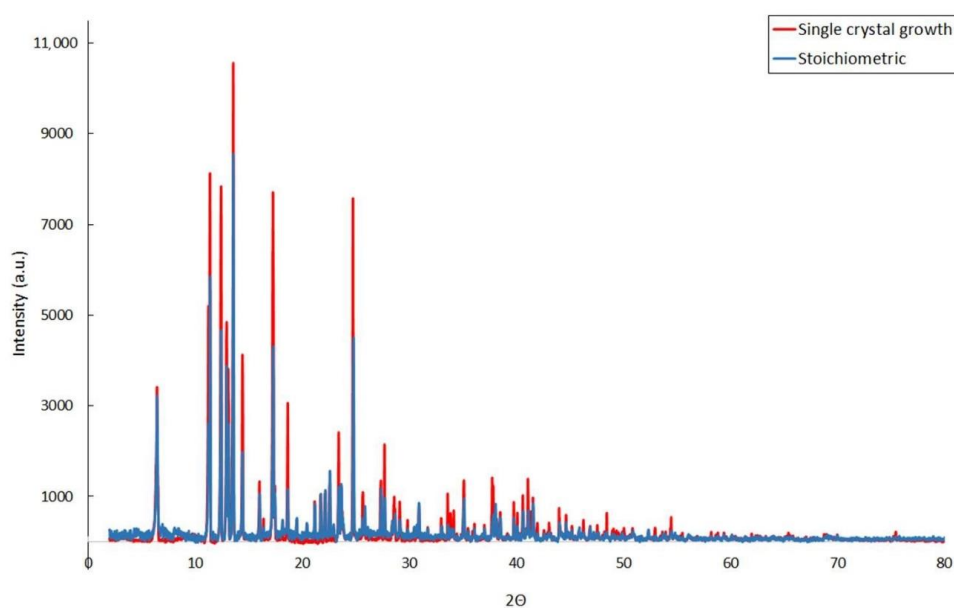


Figure 9. Superimposition of the PXRD pattern for $[\text{Cu}_2(\mu\text{-OAc})_4(\mathbf{1})]_n$ obtained from a preparative scale reaction (blue) and from the single-crystal growth experiment (red).

4. Conclusions

We have prepared and characterized compounds 1–5, which feature [1,1'-biphenyl], 4'-fluoro-[1,1'-biphenyl], 4'-chloro-[1,1'-biphenyl], 4'-bromo-[1,1'-biphenyl] and 4'-methyl-[1,1'-biphenyl] attached to the 4'-position of a 3,2':6',3''-tpy metal-binding domain. Single-crystal structures of the $[\text{Cu}_2(\mu\text{-OAc})_4\text{L}]_n$ 1D-coordination polymers with L = 1–5 have been determined. The assembly common to both $[\text{Cu}_2(\mu\text{-OAc})_4(\mathbf{1})]_n$ and $[\text{Cu}_2(\mu\text{-OAc})_4(\mathbf{2})]_n$ in which ligands 1 and 2 adopt conformation I (Scheme 2) is directed by π -stacking interactions between centrosymmetric pairs of [1,1'-biphenyl]pyridine units. Although bifurcated contacts (H...H for 1 or H...F for 2) are secondary, the two sets of interactions are interdependent, and are also dependent upon the 3,2':6',3''-tpy adopting conformation I. Increasing the steric demands of the 4'-substituent in the 1,1'-biphenyl group would force the chains (in a sheet) further apart, and if the π -stacking between pairs of [1,1'-biphenyl] pyridine units were to be retained, channels would be introduced into the lattice, reducing the packing efficiency. This hypothesis is consistent with the observed switch in ligand conformation to II (Scheme 2) on going from $[\text{Cu}_2(\mu\text{-OAc})_4(\mathbf{1})]_n$ and $[\text{Cu}_2(\mu\text{-OAc})_4(\mathbf{2})]_n$ to the analogous complexes containing 3, 4, and 5. The switch in ligand conformation leads to the dominant packing interactions involving py–py and py–biphenyl face-to-face π -stacking interactions. We are currently exploring both the coordination behavior of ligands 1–5 with other metal salts and the effects of varying the 4'-arene functionalities.

Supplementary Materials: The following are available online at <https://www.mdpi.com/2624-8549/3/1/15/s1>: Figures S1–S5: mass spectra of 1–5; Figures S6–S25: NMR spectra of 1–5; Figures S26–S35: IR spectra of ligands and coordination polymers; Figure S36: Packing diagram for $[\text{Cu}_2(\mu\text{-OAc})_4(\mathbf{3})]_n$. Figures S37–S45: PXRD figures.

Author Contributions: Project conceptualization, administration, supervision, and funding acquisition: C.E.H. and E.C.C.; investigation and data analysis: D.R. and S.N.; single-crystal X-ray diffraction and PXRD: A.P. and D.R.; manuscript writing: C.E.H. and D.R.; manuscript editing and review: all authors. All authors have read and agreed to the published version of the manuscript.

Funding: This research was partially funded by the Swiss National Science Foundation (grant number 200020_182000).

Institutional Review Board Statement: Not applicable.

Informed Consent Statement: Not applicable.

Data Availability Statement: The data presented in this study are available on request from the corresponding author. The data are not publicly accessible at present.

Acknowledgments: We gratefully acknowledge the support of the University of Basel.

Conflicts of Interest: The authors declare no conflict of interest.

References

1. Constable, E.C. The Coordination Chemistry of 2,2':6',2''-Terpyridine and Higher Oligopyridines. *Adv. Inorg. Chem. Radiochem.* **1986**, *30*, 69–121. [[CrossRef](#)]
2. Constable, E.C. 2,2':6',2''-Terpyridines: From chemical obscurity to common supramolecular motifs. *Chem. Soc. Rev.* **2007**, *36*, 246–253. [[CrossRef](#)] [[PubMed](#)]
3. Schubert, U.S.; Hofmeier, H.; Newkome, G.R. *Modern Terpyridine Chemistry*; Wiley-VCH: Weinheim, Germany, 2006; ISBN 978-3-527-31475-1.
4. Wei, C.; He, Y.; Shi, X.; Song, Z. Terpyridine-metal complexes: Applications in catalysis and supramolecular chemistry. *Coord. Chem. Rev.* **2019**, *385*, 1–19. [[CrossRef](#)]
5. Schubert, U.S.; Winter, A.; Newkome, G.R. *Terpyridine-Based Materials: For Catalytic, Optoelectronic and Life Science Applications*; Wiley-VCH: Weinheim, Germany, 2011; ISBN 9783527330386.
6. Constable, E.C. Expanded ligands: An assembly principle for supramolecular chemistry. *Coord. Chem. Rev.* **2008**, *252*, 842–855. [[CrossRef](#)]
7. Chakraborty, S.; Newkome, G.R. Terpyridine-based metallosupramolecular constructs: Tailored monomers to precise 2D-motifs and 3D-metallocages. *Chem. Soc. Rev.* **2018**, *47*, 3991–4016. [[CrossRef](#)] [[PubMed](#)]

8. Housecroft, C.E.; Constable, E.C. The Terpyridine Isomer Game: From Chelate to Coordination Network Building Block. *Chem. Commun.* **2020**, *56*, 10786–10794. [[CrossRef](#)]
9. Kröhnke, F. Syntheses Using Pyridinium Salts. *Angew. Chem. Int. Ed.* **1963**, *2*, 225. [[CrossRef](#)]
10. Wang, J.; Hanan, G.S. A facile route to sterically hindered and non-hindered 4'-aryl-2,2':6',2''-terpyridines. *Synlett* **2005**, 1251–1254. [[CrossRef](#)]
11. Sato, S.; Murase, T.; Fujita, M. Self-Assembly of Coordination Cages and Spheres. In *Supramolecular Chemistry: From Molecules to Nanomaterials*; Gale, P.A., Steed, J.W., Eds.; Wiley-Blackwell: Oxford, UK, 2012. [[CrossRef](#)]
12. Rocco, D.; Prescimone, A.; Constable, E.C.; Housecroft, C.E. Switching the conformation of 3,2':6',3''-tpy domains in 4'-(4-*n*-alkyloxyphenyl)-3,2':6',3''-terpyridines. *Molecules* **2020**, *25*, 3162. [[CrossRef](#)]
13. Rocco, D.; Manfroni, G.; Prescimone, A.; Klein, Y.M.; Gawryluk, D.J.; Constable, E.C.; Housecroft, C.E. Single and double-stranded 1D-coordination polymers with 4'-(4-alkyloxyphenyl)-3,2':6',3''-terpyridines and {Cu₂(μ-OAc)₄} or {Cu₄(μ₃-OH)₂(μ-OAc)₂(μ₃-OAc)₂(AcO-κO)₂} motifs. *Polymers* **2020**, *12*, 318. [[CrossRef](#)]
14. Rocco, D.; Prescimone, A.; Constable, E.C.; Housecroft, C.E. Straight versus branched chain substituents in 4'-(butoxyphenyl)-3,2':6',3''-terpyridines: Effects on (4,4) coordination network assemblies. *Polymers* **2020**, *12*, 1823. [[CrossRef](#)] [[PubMed](#)]
15. Rocco, D.; Prescimone, A.; Constable, E.C.; Housecroft, C.E. Directing 2D-coordination networks: Combined effects of a conformationally flexible 3,2':6',3''-terpyridine and chain length variation in 4'-(4-*n*-alkyloxyphenyl) substituents. *Molecules* **2020**, *25*, 1663. [[CrossRef](#)] [[PubMed](#)]
16. Granifo, J.; Gavino, R.; Freire, E.; Baggio, R. The new sulphur-containing ligand 4'-(4-methylthiophenyl)-3,2':6',3''-terpyridine (L1) and the supramolecular structure of the dinuclear complex [Zn₂(μ-L1)(acac)₄] (acac = acetylacetonato): The key role of non-covalent S...O contacts and C-H...S hydrogen bonds. *J. Mol. Struct.* **2011**, *1006*, 684–691. [[CrossRef](#)]
17. Henling, L.M.; Marsh, R.E. Some more space-group corrections. *Acta Crystallogr.* **2014**, *C70*, 834–836. [[CrossRef](#)]
18. Granifo, J.; Vargas, M.; Garland, M.T.; Ibanez, A.; Gavino, R.; Baggio, R. The novel ligand 4'-phenyl-3,2':6',3''-terpyridine (L) and the supramolecular structure of the dinuclear complex [Zn₂(μ-L)(acac)₄]·H₂O (acac = acetylacetonato). *Inorg. Chem. Comm.* **2008**, *11*, 1388–1391. [[CrossRef](#)]
19. Klein, Y.M.; Lanzilotto, A.; Prescimone, A.; Krämer, K.W.; Decurtins, S.; Liu, S.-X.; Constable, E.C.; Housecroft, C.E. Coordination behaviour of 1-(3,2':6',3''-terpyridin-4'-yl)ferrocene: Structure and magnetic and electrochemical properties of a tetracopper dimetallomacrocyclic. *Polyhedron* **2017**, *129*, 71–76. [[CrossRef](#)]
20. Zhao, M.; Tan, J.; Su, J.; Zhang, J.; Zhang, S.; Wu, J.; Tian, Y. Syntheses, crystal structures and third-order nonlinear optical properties of two series of Zn(II) complexes using the thiophene-based terpyridine ligands. *Dyes Pigments* **2016**, *130*, 216–225. [[CrossRef](#)]
21. Zhang, L.; Li, C.-J.; He, J.-E.; Chen, Y.-Y.; Zheng, S.-R.; Fan, J.; Zhang, W.-G. Construction of New Coordination Polymers from 4'-(2,4-disulfophenyl)-3,2':6',3''-terpyridine: Polymorphism, pH-dependent syntheses, structures, and properties. *J. Solid State Chem.* **2016**, *233*, 244–254. [[CrossRef](#)]
22. Cheng, Y.; Yang, M.-L.; Hu, H.-M.; Xu, B.; Wang, X.; Xue, G. Syntheses, structures and luminescence for zinc coordination polymers based on a multifunctional 4'-(3-carboxyphenyl)-3,2':6',3''-terpyridine ligand. *J. Solid State Chem.* **2016**, *239*, 121–130. [[CrossRef](#)]
23. Wang, T.-T.; Zhang, J.-L.; Hu, H.-M.; Cheng, Y.; Xue, L.-L.; Wang, X.; Wang, B.-Z. Syntheses, structures and luminescent properties of Zn/Cd coordination polymers based on 4'-(2-carboxyphenyl)-3,2':6',3''-terpyridine. *Polyhedron* **2018**, *151*, 43–50. [[CrossRef](#)]
24. Lufei, X.; Yupeng, T. CSD Refcode VUKMOF. In *CSD Communication CCDC 1407410*; The Cambridge Crystallographic Data Centre (CCDC): Cambridge, UK, 2015.
25. Liu, C.; Ding, Y.-B.; Shi, X.-H.; Zhang, D.; Hu, M.-H.; Yin, Y.-G.; Li, D. Interpenetrating Metal–Organic Frameworks Assembled from Polypyridine Ligands and Cyanocuprate Catenations. *Cryst. Growth Des.* **2009**, *9*, 1275–1277. [[CrossRef](#)]
26. Li, L.; Zhang, Y.Z.; Yang, C.; Liu, E.; Golen, J.A.; Zhang, G. One-dimensional copper(II) coordination polymers built on 4'-substituted 4,2':6',4''- and 3,2':6',3''-terpyridines: Syntheses, structures and catalytic properties. *Polyhedron* **2016**, *105*, 115–122. [[CrossRef](#)]
27. Köberl, M.; Cokoja, M.; Herrmann, W.A.; Kühn, F.E. From molecules to materials: Molecular paddle-wheel synthons of macromolecules, cage compounds and metal-organic frameworks. *Dalton Trans.* **2011**, *40*, 6834–6859. [[CrossRef](#)] [[PubMed](#)]
28. Constable, E.C.; Housecroft, C.E.; Neuburger, M.; Schönle, J.; Vujovic, S.; Zampese, J.A. Molecular recognition between 4'-(4-biphenyl)-4,2':6',4''-terpyridine domains in the assembly of d⁹ and d¹⁰ metal ion-containing one-dimensional coordination polymers. *Polyhedron* **2013**, *60*, 120–129. [[CrossRef](#)]
29. Constable, E.C.; Housecroft, C.E.; Vujovic, S.; Zampese, J.A.; Crochet, A.; Batten, S.R. Do perfluoroarene...arene and C-H...F interactions make a difference to 4,2':6',4''-terpyridine-based coordination polymers? *CrystEngComm* **2013**, *15*, 10068–10078. [[CrossRef](#)]
30. Software for the Integration of CCD Detector System Bruker Analytical X-ray Systems, Bruker axis, Madison, WI (after 2013).
31. Sheldrick, G.M. ShelXT-Integrated space-group and crystal-structure determination. *Acta Cryst.* **2015**, *A71*, 3–8. [[CrossRef](#)] [[PubMed](#)]
32. Dolomanov, O.V.; Bourhis, L.J.; Gildea, R.J.; Howard, J.A.K.; Puschmann, H. Olex2: A Complete Structure Solution, Refinement and Analysis Program. *J. Appl. Cryst.* **2009**, *42*, 339–341. [[CrossRef](#)]
33. Sheldrick, G.M. Crystal Structure Refinement with ShelXL. *Acta Cryst.* **2015**, *C27*, 3–8. [[CrossRef](#)]

34. Palatinus, L.; Chapuis, G. Superflip-A Computer Program for the Solution of Crystal Structures by Charge Flipping in Arbitrary Dimensions. *J. Appl. Cryst.* **2007**, *40*, 786–790. [[CrossRef](#)]
35. Palatinus, L.; Prathapa, S.J.; van Smaalen, S. EDMA: A Computer Program for Topological Analysis of Discrete Electron Densities. *J. Appl. Cryst.* **2012**, *45*, 575–580. [[CrossRef](#)]
36. Macrae, C.F.; Sovago, I.; Cottrell, S.J.; Galek, P.T.A.; McCabe, P.; Pidcock, E.; Platings, M.; Shields, G.P.; Stevens, J.S.; Towler, M.; et al. Mercury 4.0: From visualization to analysis, design and prediction. *J. Appl. Cryst.* **2020**, *53*, 226–235. [[CrossRef](#)] [[PubMed](#)]
37. LeBail, A.; Duroy, H.; Fourquet, J.L. Ab-initio structure determination of LiSbWO_6 by X-ray powder diffraction. *Mater. Res. Bull.* **1988**, *23*, 447–452. [[CrossRef](#)]
38. Pawley, G.S. Unit-cell refinement from powder diffraction scans. *J. Appl. Cryst.* **1981**, *14*, 357–361. [[CrossRef](#)]
39. Rodríguez-Carvajal, J. Recent Advances in Magnetic Structure Determination by Neutron Powder Diffraction. *Physica B* **1993**, *192*, 55–69. [[CrossRef](#)]
40. Roisnel, T.; Rodríguez-Carvajal, J. WinPLOTR: A Windows tool for powder diffraction patterns analysis Materials Science Forum. In Proceedings of the Seventh European Powder Diffraction Conference (EPDIC 7), Barcelona, Spain, 20–23 May 2000; pp. 118–123.
41. *Spartan '18 Version 1.4.4*; Wavefunction Inc.: Irvine, CA, USA, 2019.
42. Bienz, S.; Bigler, L.; Fox, T.; Meier, H. *Spektroskopische Methoden in der Organischen Chemie*, 9th ed.; Thieme: Stuttgart, Germany, 2016; ISBN 9783135761091.
43. Janiak, C. A critical account on π - π stacking in metal complexes with aromatic nitrogen-containing ligands. *J. Chem. Soc. Dalton Trans.* **2000**, 3885–3896. [[CrossRef](#)]